JGR Solid Earth

RESEARCH ARTICLE
10.1029/2021JB022678

Effects of a Weak Lower Crust on the Flexure of Continental Lithosphere

Ashley Bellas[1] and Shijie Zhong[1]

[1]Department of Physics, University of Colorado Boulder, Boulder, CO, USA

Key Points:

- In continental settings with a weak lower crust, the cubic rule, $T_e = (T_{e1}^3 + T_{e2}^3)^{1/3}$, is consistent with a transient flexural solution, only
- The steady state flexure of a multilayer lithosphere is consistent with that predicted by the upper competent crust, or $T_e = T_{e1}$
- This new rule, $T_e = T_{e1}$, becomes relevant on short geologic timescales and improves the fit to observations (e.g., at Northern Tien Shan)

Correspondence to:

A. Bellas,
Ashley.bellas@colorado.edu

Citation:

Bellas, A., & Zhong, S. (2021). Effects of a weak lower crust on the flexure of continental lithosphere. *Journal of Geophysical Research: Solid Earth*, *126*, e2021JB022678. https://doi.org/10.1029/2021JB022678

Received 28 JUN 2021
Accepted 22 SEP 2021

Abstract Previous studies of flexure in continental settings assert that the elastic thickness of a multilayer lithosphere is controlled by the mechanically competent layer thicknesses only, following a cubic rule. More specifically, the cubic rule states $T_e = (T_{e1}^3 + T_{e2}^3 + \ldots T_{en}^3)^{1/3}$, where T_e is the total elastic thickness, and T_{ei} is the elastic thickness of each competent layer. However, it is not necessarily clear that T_e should be insensitive to the properties of intermediate weak layers (e.g., a weak lower crust) which may act to decouple the surface load from lower competent layers. To test this idea, we formulate 2D viscoelastic loading models with layered viscosity to compute the fully dynamic, time-dependent response of a multilayer lithosphere with a weak lower crust. Results show that the flexural response of a multilayer lithosphere to a surface load is initially consistent with the cubic rule. However, this solution is transient because the stress associated with the load cannot be transmitted through the weak lower crust on long timescales. Stress in the mantle lithosphere relaxes with time and eventually does not support the load at all due to the decoupling effect of flow in the weak lower crust. The steady state flexure of a multilayer lithosphere is controlled solely by the mechanically competent upper crust such that $T_e = T_{e1}$, and this new rule is the major finding of this study. Our new findings now explain small estimates of T_e in continental settings with thick mantle lithosphere such as the Northern Tien Shan, which previously, were poorly explained by the cubic rule.

Plain Language Summary Previous studies of flexure assume that in continental settings with a weak lower crust, surface flexure is controlled by the combined strength of upper and lower competent layers following a cubic rule. In particular, they assume that the total elastic thickness is given by $T_e = (T_{e1}^3 + T_{e2}^3)^{1/3}$. However, it is not necessarily clear how T_e may depend on the intermediate weak layer. In this study, we test whether the response of a multilayer lithosphere is consistent with the cubic rule using viscoelastic loading models. Results show that the response of a multilayer lithosphere is initially consistent with the cubic rule, but that flow in the intermediate weak layer acts to decouple the lower competent layer from the surface load, such that surface flexure is ultimately controlled by the upper competent layer, only (i.e., $T_e = T_{e1}$). This new result explains small estimates of T_e in continental settings with thick mantle lithosphere such as the Northern Tien Shan Mountains, which were previously poorly understood.

1. Introduction

The rheology of continental lithosphere controls seismicity, orogeny, basin-formation in continents, and is partially responsible for the bimodal recycling of Earth's surface wherein continental lithosphere may be older than several Ga while oceanic lithosphere is generally younger than 200 Ma. Because of the sensitivity of lithospheric rheology to temperature and composition, increased crustal thickness may give rise to an intermediate weak layer (i.e., weak lower crust) (Bird, 1991; Chen & Molnar, 1983), which may have a significant impact on the tectonics of orogenic regions such as Tibet (Clark & Royden, 2000; Royden et al., 1997). Lithospheric rheology is frequently investigated in mineral physics experiments (Goetze & Evans, 1979) and inferred from field observations of radial seismic anisotropy (e.g., Shapiro et al., 2004) and surface wave tomography (Shen et al., 2013) which show that crustal rocks (e.g., quartz, diabase) may become extremely weak for conditions under which adjacent lithospheric mantle rocks remain much stronger (e.g., olivine). Lithospheric rheology is also frequently constrained by observations of flexure in response to surface loads such as mountains ranges, plateaus, basins, and glacial isostatic adjustment (Watts, 2001). However, it is not necessarily clear what effects an intermediate weak layer may have on lithospheric flexure and what

© 2021. American Geophysical Union. All Rights Reserved.

implications this may have for constraints on continental rheology. In the following, we briefly review the origins of the cubic rule.

In flexural studies, the effective elastic thickness (T_e) of the lithosphere is estimated based on a comparison of observed flexure to that predicted for an elastic plate subject to an estimated surface load (i.e., the elastic plate model) (e.g., McNutt, 1984; Turcotte & Schubert, 1982; Walcott, 1970). Previous studies have extended the elastic plate model to include anelastic yielding in the yield stress envelope (YSE) method (Garcia et al., 2019; McNutt & Menard, 1982; Mueller & Phillips, 1995) in which the bending moment of a yielding plate is estimated by vertically integrating an inferred stress profile based on laboratory-derived rheological parameters,

$$M_0 = \int \sigma_{xx}\left(z - z_n\right)dz, \tag{1}$$

in which σ_{xx} is the differential bending stress, z is depth, and z_n the depth of the neutral plane. Then, to solve T_e of the yielding plate, the bending moment based on Equation 1 is equated to the bending moment of a purely elastic plate

$$M_0 = \frac{\kappa E}{12\left(1-\nu^2\right)}T_e^3, \tag{2}$$

in which κ is surface curvature, E is Young's modulus, and υ is Poisson's ratio.

In general, the integral in Equation 1 is applied across the entire depth of the lithosphere and previous studies have asserted that because integrating over weak zones contributes little to the bending moment, the total bending moment of a multilayer lithosphere should simply be the sum of the bending moments in each mechanically competent layer. Therefore, because the bending moment in each competent layer is proportional to the elastic thickness-cubed (Equation 2), previous studies asserted that the effective elastic thickness T_e of a multilayer lithosphere should be given by (e.g., Burov, 2015; Burov & Diament, 1995),

$$T_e = \left(\sum_{i=1}^{n} T_{ei}^3\right)^{\frac{1}{3}}, \tag{3}$$

in which n is the number of mechanically competent layers, and T_{ei} is the elastic thickness of each competent layer, i. Equation 3 expresses the cubic rule for T_e which we will test in the following study.

According to the cubic rule, the flexure of a multilayer lithosphere is assumed to be entirely determined by the competent layer thicknesses (e.g., Burov, 2015; Burov & Diament, 1995). However, it is not necessarily clear how the dynamics of a multilayer lithosphere may be dependent on the properties of intermediate weak layers. For example, curvature of the upper mechanically competent layer may exceed that of a lower competent layer if the latter is decoupled from a surface load by an intermediate weak layer, and the degree of decoupling may be sensitive to the weak layer viscosity and geometry. The significance of competent layers being subject to different curvature is that curvature controls the proportionality relation between elastic thickness and the bending moment. In other words, summing the bending moments of multiple competent layers in a multilayer lithosphere (Equation 2) simplifies to the cubic rule if and only if curvature is constant across layers. We find it pertinent to test whether surface stresses are indeed transmitted to deep mechanically competent layers which may be decoupled from the surface by intermediate weak layers, especially because the cubic rule has been broadly applied in flexural studies but relies on an assumption that has not yet been verified (e.g., Burov, 2015; Burov & Diament, 1995; McNutt et al., 1988).

In this study, we test whether the cubic rule (Equation 3) is valid for geologically relevant rheological structures. We hypothesize that the weak lower crust may act as a decoupling layer that imposes significant influence on the flexural response of the lithosphere to surface loads and the predicted elastic thickness. We assemble 2D viscoelastic loading models subject to surface loads to directly test whether a plate with an intermediate weak layer responds similarly to a plate with total elastic thickness based on the cubic rule. Both analytic and numerical solutions are available for viscoelastic deformation of a medium with layered viscosity and both are implemented herein. The models of this study also represent the first fully dynamic assessment of the effects of a weak intermediate layer on flexure.

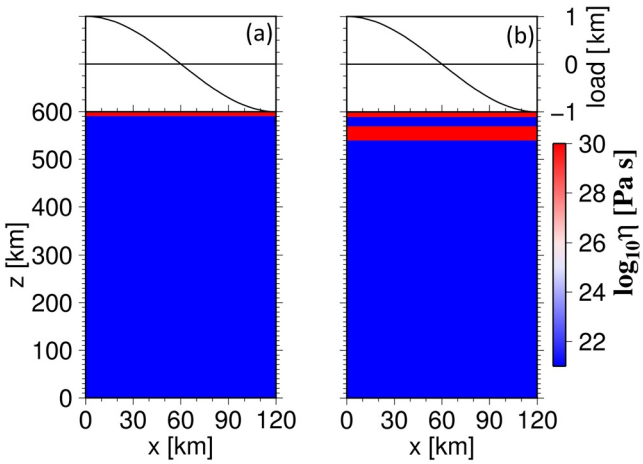

Figure 1. Viscosity and the load. The viscosity structure and the surface load, $h(x)$, for (a) Case 0a, a two-layer model with $T_e = 10$ km, and (b) Case 1, a four-layer model with $T_{e1} = 10$ km, $T_{e2} = 30$ km, and weak layer thickness equal to 20 km. Note that the vertical sides are subject to a reflecting boundary condition such that solutions are effectively periodic. The top surface is free and deformable, and the bottom surface is free-slip.

2. Methods

The response of a viscoelastic medium to a surface load may be solved analytically provided the viscosity is limited to vertically stratified layers only, while numerical solutions are required for more complex viscosity structures. Both analytic and numerical models are used in this study and in the following, we introduce the properties that apply to both. Both models solve the time-dependent response of an incompressible Maxwellian medium to a surface load in 2D Cartesian geometry. The surface boundary is a free and deformable density interface, while the vertical side and bottom boundaries are subject to the free-slip condition. The entire domain has uniform mantle density, uniform elastic properties, and the viscosity is layered (models have two or four distinct viscosity layers).

The governing equations for an incompressible medium are conservation of mass and momentum (e.g., Zhong, 1997)

$$u_{i,i} = 0, \tag{4}$$

$$\tau_{ij,j} - \left(\rho g u_2\right)_i = 0, \tag{5}$$

in which u_i is displacement, τ_{ij} is the stress tensor, ρ is density, g is acceleration due to gravity, u_2 is the displacement in the vertical dimension, and we use subscript notation where subscripts following a comma denote a spatial derivative. The rheology of a Maxwellian medium is derived from elastic and viscous deformation combined in series (e.g., Zhong, 1997)

$$\tau_{ij} + \frac{\eta}{\mu}\dot{\tau}_{ij} = p\delta_{ij} + \eta\dot{\epsilon}_{ij}, \tag{6}$$

in which η is viscosity, μ is the shear modulus, $\dot{\tau}_{ij}$ is the stress rate tensor, p is pressure, and $\dot{\epsilon}_{ij}$ is the strain rate tensor. An important timescale known as the Maxwell time, $\tau_M = \eta/\mu$, controls the timescale on which viscoelastic deformation occurs.

The surface is subject to a time-independent topographical load, $\sigma_0 = \rho g h(x)$, in which ρ is mantle density, and the load height is given by

$$h\left(x\right) = h_0 \cos\frac{2\pi x}{\lambda}, \tag{7}$$

in which h_0 is the load amplitude, x is the horizontal coordinate, and λ is the load wavelength. The domain-width is equal to the half-wavelength of the load (120 km in most cases), and the domain-depth is 600 km (Figure 1). In the following subsections, we describe the differing aspects of the analytic and numerical models separately. We will also present some results based on the elastic plate model which is well documented in other sources and not reproduced here (e.g., Turcotte & Schubert, 1982).

2.1. The Analytic Viscoelastic Loading Model

The 2D analytic viscoelastic loading model was developed by Zhong (1997) and includes the propagator matrix method (e.g., Hager & O'Connell, 1981). It is formulated in three important steps: (a) the Laplace transform is applied to express the governing equations in the spectral domain; (b) the unknowns are solved in the Laplace domain following the propagator matrix method; and (c) the reverse Laplace transform is applied to transform variables back into the time domain. All horizontal dependencies of model parameters are expressed in terms of Fourier series for a given wavelength, λ. The result of this solution method is that the flexural response of the free surface is controlled by eigenmodes of deformation, and the number of eigenmodes that contribute to the total solution is given by the number of density and viscosity interfaces in the model. One eigenmode is contributed to the total solution for each deformable density interface (i.e., the surface in our models), and two eigenmodes are added for each internal viscosity interface. For example, the surface flexure will be governed by three distinct eigenmodes in a model that contains one deformable boundary and one internal viscosity interface.

Table 1
Characteristic Times and Amplitudes of Analytic Eigenmodes

i	$\tau^{(i)}$ (years)	$A_0^{(i)}/h_0$
	Case 0a, $T_e = 10$ km	
1	2.93942E+03	3.67367E-04
2	4.48776E+04	8.47010E-01
3	1.09837E+12	1.33900E-01
	Case 0b, $T_e = 30$ km	
1	2.00047E+03	2.17841E-04
2	1.26957E+04	1.92528E-01
3	4.49852E+12	7.88532E-01
	Case 0c, $T_e = 60$ km	
1	1.90853E+03	3.31997E-05
2	3.76460E+03	2.84508E-02
3	2.01519E+13	9.52794E-01
	Case 1, $T_{e1} = 10$ km, $T_{e2} = 30$ km	
1	9.53011E+02	2.16342E-06
2	1.30260E+03	2.54284E-03
3	2.11170E+03	3.29208E-03
4	2.92738E+03	1.76302E-04
5	2.32704E+04	1.73081E-01
6	2.31675E+06	6.68283E-01
7	1.09837E+12	1.33901E-01
	Case 1a, $T_e = 30.3659$ km	
1	1.99701E+03	2.13693E-04
2	1.24107E+04	1.87049E-01
3	4.61826E+12	7.94015E-01

Note. i is the eigenmode number, $\tau^{(i)}$ is the characteristic timescale, $A_0^{(i)}$ is the characteristic amplitude, and h_0 is the amplitude of the load.

The time-dependent amplitude of surface flexure expressed in terms of eigenmodes is given

$$w_0(t) = \sum_{i=1}^{n} A_0^{(i)} \exp\left[-\frac{t}{\tau^{(i)}}\right] - h_0, \tag{8}$$

in which $A_0^{(i)}$ is the characteristic amplitude of each eigenmode, i, and $\tau^{(i)}$ the characteristic timescale of each eigenmode, i. The horizontal dependence (x) is sinusoidal with wavelength equal to that of the load (i.e., $\cos(2\pi x/\lambda)$). Results will generally be presented in terms of the load-normalized amplitude of flexure, $w_0(t)/h_0$.

It is clear from Equation 8 that as t goes to infinity, the normalized flexural response approaches −1, which represents complete isostatic compensation of the surface load. Meanwhile, at $t = 0$, the initial flexure is expressed

$$\frac{w_0(t=0)}{h_0} = \sum_{i=1}^{n} \frac{A_0^{(i)}}{h_0} - 1, \tag{9}$$

which represents the instantaneous elastic response which is generally <0 (i.e., opposite sign to the surface load h_0) since the sum of the characteristic amplitudes (i.e., $\Sigma_{i-1}{}^{n} A_0^{(i)}/h_0$) is a constant generally <1. As time evolves, eigenmodes decay on timescales defined by the characteristic timescale, $\tau^{(i)}$ (Equation 8).

2.2. The Numerical Viscoelastic Loading Model

The numerical viscoelastic loading model was initially developed by Zhong et al. (2003) using an incremental displacement formulation such that the matrix equations can ultimately be solved by the same solvers as are applied in viscous flow models for mantle convection (i.e., the Uzawa algorithm as implemented in Citcom). The solutions include 2D time-dependent displacement, stress, strain rate, and surface flexure, and the grid is Lagrangian to best accommodate the viscoelastic deformation. The same finite element code, CitcomSVE, has been applied with 3D spherical geometry to post-glacial rebound problems (Paulson et al., 2005; Zhong et al., 2003), and with 3D Cartesian geometry to model volcanic loading at ocean islands and seamounts (Bellas et al., 2020; Bellas & Zhong, 2021; Zhong & Watts, 2013).

Our 2D Cartesian numerical models employ a finite element grid with 25 grid points in the horizontal direction and 81 grid points in the vertical direction. The domain width is varied based on the half-wavelength of the load (120 km for most cases), and the domain depth is 600 km in all cases. Vertical grid refinement is applied near the surface such that the vertical resolution is 2.5 km in the upper 100 km. The time-evolution of the numerical model is resolved by time steps $\Delta t = \tau_M/2$, where $\tau_M = \eta_0/\mu \sim 950$ years is the Maxwell time defined by the minimum viscosity in the model (10^{21} Pa s).

3. Results

In the following, we first present results for a simple, two-layer viscosity model to illustrate how eigenmodes control the analytic solution of surface flexure. We then present results for a series of four-layer models to systematically test the validity of the cubic rule (Equation 3).

3.1. Single-Layer Lithospheres

In Case 0a, the viscosity is 10^{30} Pa s in the upper 10 km, and 10^{21} Pa s in the lower 590 km, and the surface is subject to a load with 1 km amplitude and 120 km half-wavelength (i.e., $\lambda = 240$ km). (Figure 1a, Table 1). The Maxwell time ($\tau_M = \eta/\mu$) associated with the high-viscosity layer is $\sim 10^{12}$ years such that negligible viscous stress relaxation occurs on tectonically reasonable timescales (e.g., <1 Gyr), so we refer to this model as having elastic thickness $T_e = 10$ km.

The surface flexure is governed by three eigenmodes which have characteristic timescales $\tau^{(1)} = 2.93942 \times 10^3$ years, $\tau^{(2)} = 4.48776 \times 10^4$ years, and $\tau^{(3)} = 1.09837 \times 10^{12}$ years, and normalized characteristic amplitudes $A_0^{(1)}/h_0 = 3.67367 \times 10^{-4}$, $A_0^{(2)}/h_0 = 0.847010$, and $A_0^{(3)}/h_0 = 0.133900$ (Table 1). The exceedingly large characteristic time of the third eigenmode, $\tau^{(3)} = 1.09837 \times 10^{12}$ years, is consistent with the Maxwell time for large lithospheric viscosity (10^{30} Pa s), while the first two modes are associated with much shorter timescales (10^3–10^4 years) that are consistent with the Maxwell time for mantle viscosity (10^{21} Pa s). Therefore, the first two eigenmodes manifest the effects of viscous stress relaxation in the mantle, and the third eigenmode manifests the effects of viscous stress relaxation in the lithosphere on surface flexure.

At $t = 0$ in Case 0a, the deflection of the surface is associated with the purely elastic response of the entire domain and has very small amplitude $w_0(t = 0)/h_0 = -0.0187$ (Figure 2a) (refer to Equation 9 for a simple relation between this amplitude and the eigenmodes). At $t \sim 10^4$ years (i.e., $t \sim \tau^{(2)}$), mantle stresses begin to relax, lithospheric stresses increase, and the amplitude of flexure increases due to the evolution of the second eigenmode (Figures 2a and 2b). In general, the second eigenmode is of great significance because it represents the vertical displacement of the Earth's surface that results from the viscous relaxation of stress in the mantle and the elastic support of stress in the lithosphere, which may be modeled and compared with observations to constrain mantle viscosity (e.g., glacial isostatic adjustment). After $t \sim 10^5$ years (i.e., $t >> \tau^{(2)}$), the second eigenmode has completely decayed (i.e., viscous stress relaxation in the mantle has reached steady state) and the flexure has reached a steady state with amplitude $w_0(t)/h_0 = -0.866$ (Figure 2b). The amplitude of the steady state flexure is given by $1-A_0^{(3)}/h_0 = -0.866$ for t that is significantly larger than $\tau^{(2)}$ or $\sim 10^5$ years but less than $\tau^{(3)}$ or $\sim 10^{12}$ years (Equation 8), and represents the *lithospheric mode* (i.e., the elastic response of the lithosphere) which is consistent with the flexure computed by the elastic plate model (e.g., Turcotte & Schubert, 1982). As time approaches $\tau^{(3)}$ or $t \sim 10^{12}$ years, lithospheric stress starts to relax viscously (i.e., the third eigenmode starts to decay), and surface flexure eventually reaches -1 at which point lithospheric stress is fully relaxed and the system is in a state of complete isostatic compensation (Figure 2b, Equation 8). Of key importance is that the lithospheric mode (i.e., the steady state flexure between $\sim 10^5$ and $\sim 10^{12}$ years) is controlled by the third eigenmode (e.g., $1-A_0^{(3)}/h_0 = -0.866$).

The time-dependent solutions of the flexure based on numerical viscoelastic models agree with analytical solutions extremely well (Figures 2a and 2b), as expected (Zhong et al., 2003; Zhong & Watts, 2013). The numerical solution is computed up to the lithospheric mode, only, for computational efficiency and since viscous relaxation of the lithosphere is not particularly relevant to observations of flexure. Good agreement with the lithospheric mode of the analytic viscoelastic solution is also achieved by the elastic plate model (Figures 2a and 2b).

We also present solutions for two-layer models with $T_e = 30$ km (Case 0b and Figures 2c and 2d) and $T_e = 60$ km (Case 0c and Figures 2e and 2f). The dynamics are broadly similar to those of Case 0a with $T_e = 10$ km, except that the amplitudes and timescales of the responses differ (Figure 2 and Table 1). As T_e increases, $\tau^{(1)}$ and $\tau^{(2)}$ decrease slightly, $\tau^{(3)}$ increases slightly, and $A_0^{(3)}$ increases significantly at the expense of other two modes (Table 1 and Figure 2). Note also that the numerical viscoelastic solutions always agree with the analytical viscoelastic solutions, but the agreement achieved by the elastic plate model degrades for larger T_e because the thin plate approximation breaks down for increasing T_e.

3.2. Multilayer Lithospheres

In this subsection, we test whether the flexural response of a multi-layer lithosphere is consistent with the cubic rule (e.g., Burov, 2015). Results are derived primarily from analytic models which predict surface flexure based on eigenmodes, and results from numerical models are presented secondarily to investigate the evolution of internal stresses.

3.2.1. Effects of an Intermediate Weak Layer

First, we test Case 1, a four-layer model with a total lithospheric thickness of 60 km within which there are three layers with thicknesses 10, 20, and 30 km from the top to bottom, which have viscosity equal to

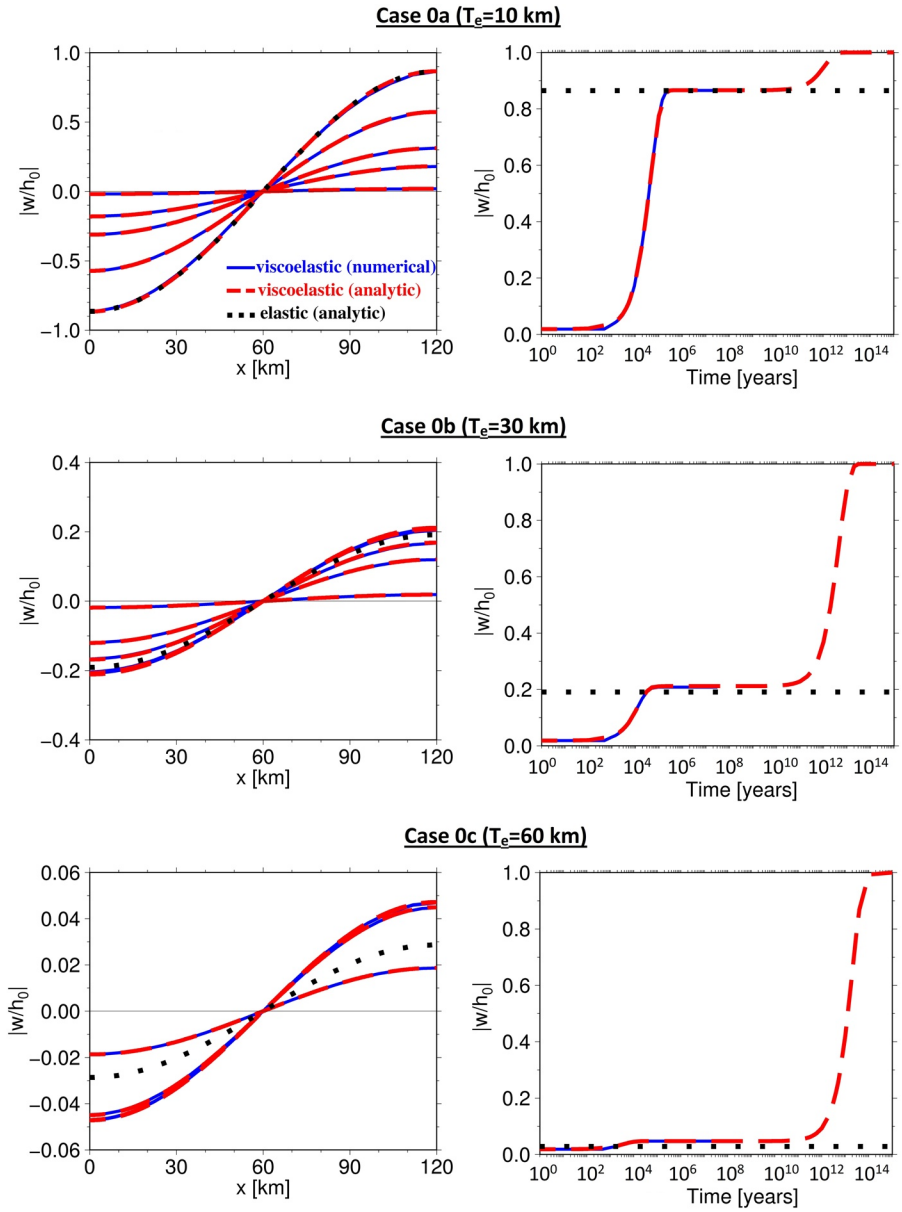

Figure 2. Time-dependent surface flexure. In the left-hand column (a, c, and e) we show the normalized surface deflection as a function of horizontal location, *x*, and time, *t* for $t = 0$, 9.5, 19.0, 47.6 kyr, and 30.4 Myr based on the numerical and analytic viscoelastic models, and the analytic elastic plate model. Note that the vertical axis limits are not constant, and the legend in (a) is relevant to all panels. In the right-hand column (b, d, and f), we show the normalized amplitude of surface deflection as a function of time. The numerical viscoelastic solution is evolved up to only ~30 Myr or the steady state elastic response of the lithosphere. The solutions based on the viscoelastic models agree well in all instances, while the elastic plate model begins to deviate from the viscoelastic solutions for large plate thickness compared to the wavelength of the load (c–f) due to breakdown of the thin plate approximation.

10^{30}, 10^{21}, and 10^{30} Pa s, respectively (Figure 1b). The high-viscosity lithospheric layers are referred to as the upper and lower mechanically competent layers. The load amplitude $h_0 = 1$ km and the load wavelength $\lambda = 240$ km.

The flexural response is controlled by seven distinct eigenmodes, as expected for a system with one deformable density interface and three internal viscosity interfaces (Table 1). The first five eigenmodes have characteristic times $\tau^{(1-5)} \leq 12.33 \times 10^4$ years, while the seventh mode has $\tau^{(7)} = 1.10 \times 10^{12}$ years. The

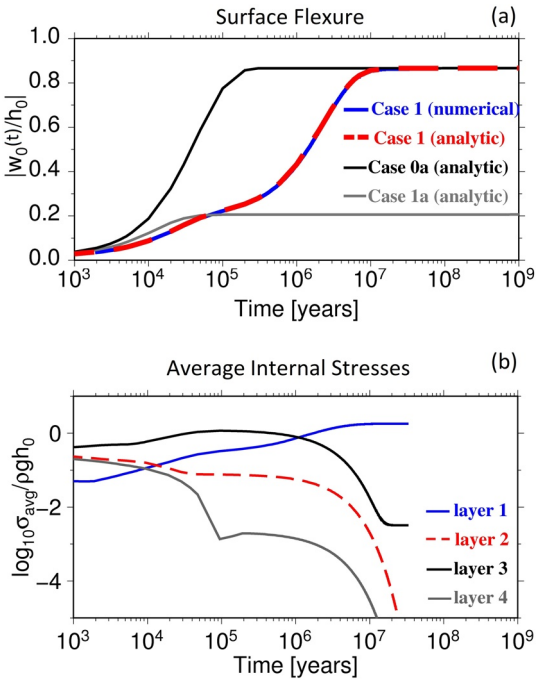

Figure 3. Time-evolution of flexure and internal stresses. (a) The load-normalized amplitude of flexure from Case 1, Case 0a, and Case 1a. (b) Stress averaged in each layer of the numerical Case 1 as a function of time, where layers are labeled 1–4 from top to bottom, such that layer 1 corresponds to the upper competent layer, layer 2 to the intermediate weak layer, layer 3 to the lower competent layer, and layer 4 to the upper 50 km of the underlying mantle. The key result presented in this figure is that flexure of the multilayer lithosphere (Case 1) deviates from the cubic rule (Case 1a) on the same timescale as stress relaxation in layers 2, 3, and 4.

characteristic timescales $\tau^{(1-5)}$ and $\tau^{(7)}$ are consistent with the Maxwell time for mantle viscosity and lithospheric viscosity, respectively. However, the sixth eigenmode with $\tau^{(6)} = 2.32 \times 10^6$ years has a distinct timescale from any of those in two-layer models, thus reflecting the effect of the intermediate weak layer. Note that the sixth eigenmode also has a relatively large amplitude $A_0^{(6)}/h_0 = 0.668$ (Table 1), indicating that this eigenmode has a dominant influence on surface flexure. Note also that $\tau^{(7)} = 1.09837 \times 10^{12}$ years and $A_0^{(7)}/h_0 = 0.133901$ are nearly identical to those of the third eigenmode in the two-layer model Case 0a with $T_e = 10$ km (Table 1), indicating a nearly identical steady state flexure arises between $\tau^{(6)} = 2.32 \times 10^6$ years and $\tau^{(7)} = 1.09837 \times 10^{12}$ in Case 1 as between $\tau^{(2)} = 4.48776 \times 10^4$ years and $\tau^{(3)} = 1.09837 \times 10^{12}$ years in Case 0a (the significance of this agreement will be made clear shortly).

Figure 3a shows the amplitude of flexure as a function of time in Case 1. For the first 10^5 years, flexure is controlled by the first five eigenmodes which have short characteristic times ($<10^5$ years) and small amplitudes (~0.2 load-normalized sum total). The dominant flexural response is centered on $\tau^{(6)} \sim 2 \times 10^6$ years and has amplitude $A_0^{(6)} \sim 0.7$ consistent with the sixth eigenmode (Table 1). After $\sim 10^7$ years, the flexure reaches a steady state with normalized amplitude $w_0(t)/h_0 = A_0^{(7)}/h_0 - 1 = -0.866$. It is not until $\tau^{(7)} \sim 1.10 \times 10^{12}$ years that the seventh eigenmode decays (Equation 8), causing lithospheric stress to relax viscously and surface flexure to approach a state of complete isostatic compensation of the load (Table 1; note that Figure 3a only displays up to 10^9 years). The numerical model accurately reproduces the analytic results up to ~30 Myr and evolves to an identical steady state surface flexure (i.e., lithospheric mode). This comparison provides a benchmark of the numerical model against analytic solutions for long timescales and a multilayer lithosphere which is, to the best of our knowledge, the first for such a benchmark.

Next, we estimate the effective elastic thickness of the multilayer lithosphere according to the cubic rule in Case 1a. Since the multilayer lithosphere contains two mechanically competent layers with $T_{e1} = 10$ km and $T_{e2} = 30$ km, we assign $T_e = (T_{e1}^3 + T_{e2}^3)^{1/3} = 30.37$ km (Table 1). The evolution of flexure in Case 1a and Case 1 are relatively consistent for $t = 0$ to $t = \sim 10^5$ years, but the results diverge after 10^5 years (Figure 3a). After 10^5 years, the flexure for the cubic Case 1a has already reached steady state with a value of ~0.2, while the flexure of the multilayer lithosphere in Case 1 begins to increase dramatically due to the evolution of the sixth eigenmode ($\tau^{(6)} \sim 2 \times 10^6$ years) (Figure 3a). As discussed earlier, the sixth eigenmode captures the effect of the intermediate weak layer and, unsurprisingly, it is the sixth eigenmode that causes the divergence of surface flexure between the multilayer lithosphere and the cubic rule. Therefore, comparison of Case 1a and Case 1 clearly demonstrates that the cubic rule fails to estimate the effective elastic thickness of a multilayer lithosphere on long timescales. To understand why the flexure of the multilayer lithosphere in Case 1 diverges from that predicted by the cubic rule in Case 1a, we analyze the time-dependent stress field from the numerical model of Case 1.

The evolution of stress in the multilayer lithosphere is presented in Figures 3b and 4. At $t = 0$, the instantaneous elastic response of the entire domain produces stress that is uniformly distributed (Figure 4). As time evolves, viscous stress relaxation occurs in the underlying mantle, and elastic stresses become concentrated in the lithosphere (Figures 4a–4e). Stresses in the intermediate weak layer and lower competent layer start to decrease after ~0.5 Myr (Figures 3b and 4e) and become a small fraction of that in the upper competent layer after ~12 Myr (Figures 4f–4h). The significance of this result is that stress relaxation in the lower layers appears to be correlated with the deviation of flexure from the cubic rule.

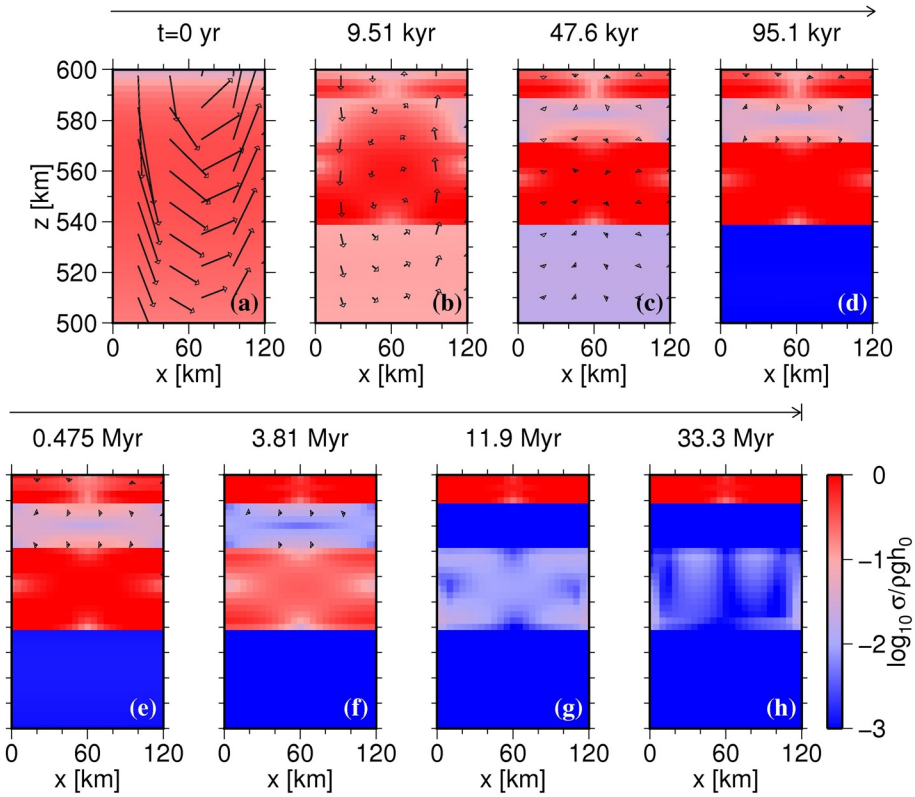

Figure 4. Time-evolution of stress in the multilayer lithosphere of Case 1. (a–h) Stress (σ) normalized by the load stress ($\rho g h_0$) and velocity vectors in the upper 100 km of the domain at various times. Flow in the intermediate weak layer decouples the lower competent layer and underlying mantle from the surface load.

The precise time-evolution of stress in the multilayer lithosphere is more easily compared with the surface flexure in Figure 3, which shows that the relaxation of stress in the lower layers occurs on the same timescale as the flexural deviation from the cubic rule (Figures 3a and 3b). These results indicate that prior to ~0.5 Myr, significant support of the surface load was provided by stresses in the lower competent layer, because the greatest amount of stress relaxation occurs in the lower competent layer between ~0.5–10 Myr, and this leads to significant increases in both the surface flexure and the stress in the upper competent layer. In addition, lateral flow and stress relaxation in the intermediate weak layer appear to accommodate stress relaxation in the lower competent layer (Figure 4). This indicates that Case 1 diverges from Case 1a because the lower competent layer becomes decoupled from the surface load by flow in the intermediate weak layer.

We hypothesize that only the uppermost competent layer is responsible for supporting surface loads on long timescales since stresses in the lower competent layer relax in Case 1. To test this hypothesis, we re-consider the two-layer model Case 0a, with $T_e = 10$ km, from Section 3.1 which has an identical lithospheric mode (i.e., $\tau^{(3)}$ and $A_0^{(3)}/h_0$) to that of Case 1 (i.e., $\tau^{(7)}$ and $A_0^{(7)}/h_0$), as pointed out earlier. Since the normalized steady state flexure, $w_0(t)/h_0 = A_0^{(3)}/h_0 - 1 = -0.866$, for Case 0a is identical to that of Case 1 with multilayer lithosphere, we thus confirm our hypothesis that the steady state flexural response of a multilayer lithosphere is identical to that of the uppermost competent layer only, due to decoupling of the lower competent layer from the surface load (Figure 3a).

In summary, we find it is not appropriate to estimate the effective elastic thickness, T_e, of a multilayer lithosphere following the cubic rule (Equation 3). Rather, the effective elastic thickness of a multilayer lithosphere is simply that of the uppermost competent layer where surface loads are applied (i.e., $T_e = T_{e1}$). Furthermore, we show that the flexural response of the multilayer lithosphere in Case 1 is governed by seven eigenmodes, and that the sixth eigenmode causes the deviation from the cubic rule. In the following,

Table 2
Model and Suite Parameter Values

Suite properties			
Suite	T_{e1} (km)	T_{e2} (km)	$(T_{e1}^3 + T_{e2}^3)^{1/3}$ (km)
1	10	30	30.3659
2, 8, 12	10	50	50.1330
3	20	50	51.0447
4, 7, 11	50	50	62.9961
5, 9, 13	10	10	12.5992
6, 10, 14	50	100	104.004

Case Properties			
Case	Weak layer thickness (km)	Weak layer viscosity (Pa s)	$\lambda/2$ (km)
b	1	1×10^{19}	25
c	2	2×10^{19}	50
d	3	3×10^{19}	120
e	4	1×10^{20}	200
f	5	2×10^{20}	400
g	10	3×10^{20}	1,000
h	15	1×10^{21}	–
i	20	2×10^{21}	–
j	25	3×10^{21}	–
k	30	1×10^{22}	–

Note. Suites of models are identified by number, and the cases within each suite are identified by letter. Within a given suite, only one of (a) the weak layer thickness, (b) weak layer viscosity, or (c) half-wavelength of the load is varied. Cases associated with the letter "a" (e.g., Case 0a, Case 1a) are two-layer and have either $T_e = (T_{e1}^3 + T_{e2}^3)^{1/3}$ or $T_e = T_{e1}$ (refer to text and Table 1).

we will test the sensitivity of these results, specifically the timescale and amplitude of the deviation from the cubic rule (i.e., $\tau^{(6)}$ and $A_0^{(6)}/h_0$), to properties of the lithosphere including layer thicknesses, weak layer viscosity, and the wavelength of the load.

3.2.2. Effects of the Lithospheric Layer Thicknesses

In the following, we explore the sensitivity of the results to the weak layer thickness. In Suite 1, we compute a set of models that are identical to Case 1 except the weak layer thickness is varied from 1 to 30 km (Table 2). Note that Case 1a (based on the cubic rule) is relevant to all cases in Suite 1 because T_{e1} and T_{e2} are held constant. In Figure 5a, we show that the time-dependent flexural response of Case 1 is representative of all cases in Suite 1, including an identical lithospheric mode, $A_0^{(7)}/h_0$, because $T_{e1} = 10$ km for all such cases (i.e., $w_0/h_0 = 0.866$ is the steady state flexural response) (Figure 5a). The amplitude of the deviation from the cubic rule is also identical for all cases in Suite 1, although the deviation occurs sooner for a thicker weak layer. For an intermediate weak layer thickness equal to 5 km, the cubic rule represents a reasonable approximation of the multilayer lithosphere until $t \sim 20$ Myr, while for 20 km thick weak layer (Case 1), the cubic rule can only be applied until $t \sim 0.3$ Myr (Figure 5a).

Next, we test the sensitivity of the results to different competent layer thicknesses in addition to weak layer thicknesses. In Suite 2, we increase the lower competent layer thickness T_{e2} to 50 km, and all other aspects of the models are identical to Suite 1. The results for Suite 2 are broadly the same as Suite 1 including identical steady state flexure (due to equivalent T_{e1}), and similar timescale for deviation from the cubic rule, $\tau^{(6)}$ (Figure 5b). However, in Suite 2, the amplitude of the deviation from the cubic rule, $A_0^{(6)}/h_0$, has increased because of increased T_{e2} which suppresses the flexural response based on the cubic rule (gray line

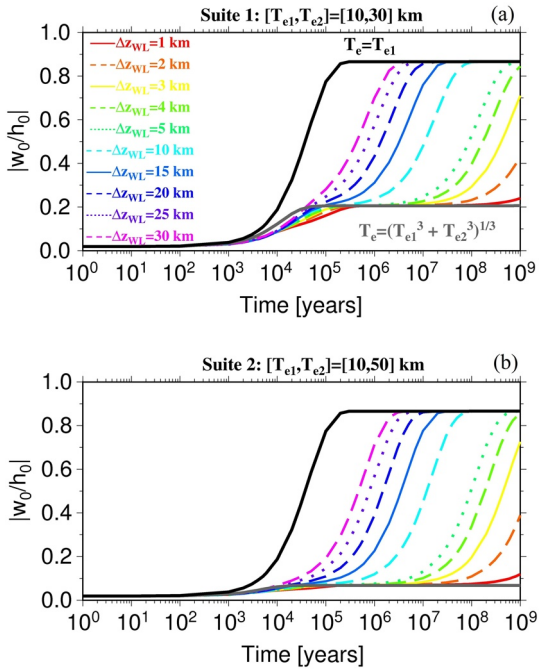

Figure 5. The normalized flexural amplitude as a function of time for varying weak layer thickness. The thickness of the weak layer, Δz_{WL}, is varied from 1 to 30 km in Suite 1 (a), and Suite 2 (b). Results are compared with two-layer models for which $T_e = T_{e1}$ (black), and the cubic rule, $T_e = (T_{e1}^3 + T_{e2}^3)^{1/3}$ (gray).

in Figure 5b), but not the eventual steady state flexural response of the multilayer lithosphere (black line in Figure 5b).

Suites 1 and 2 show that the cubic rule accurately predicts flexure during a certain time window that falls between $\tau^{(5)}$ and $\tau^{(6)}$ (Figure 5). While $\tau^{(5)}$ is controlled by mantle viscosity and always $<10^5$ years, $\tau^{(6)}$ is controlled by the intermediate weak layer and may vary from ~1 Myr to 100s of Myr (Figure 5). In the following, we define more precisely an upper bound timescale, t_u, on which the cubic rule applies. Note that the steady state flexure or lithospheric mode of a multilayer lithosphere is given by

$$w_E = A_0^{(7)}/h_0 - 1, \tag{10}$$

where $w_E = -0.866$ for all cases of Suite 1 and Suite 2 due to constant T_{e1} (i.e., the horizontal portion of the black line labeled T_e=T_{e1} in Figure 5a). Meanwhile, the steady state flexural amplitude according to the cubic rule for Suite 1 is $w_C = -0.206 = A_0^{(3)}/h_0 - 1$ (i.e., the horizontal portion of the gray line in Figure 5a). Because the steady state flexure predicted by the cubic rule is also effectively identical to the transient steady state flexure in the multilayer cases, or $w_0(t)/h_0 = A_0^{(6)}/h_0 + A_0^{(7)}/h_0 - 1$ (e.g., for Case 1, $w_C = -0.198$; Table 1), we take

$$w_C = A_0^{(6)}/h_0 + A_0^{(7)}/h_0 - 1. \tag{11}$$

where both $A_0^{(6)}$ and $A_0^{(7)}$ are constant for all cases of a given suite (i.e., the horizontal portion of the gray line labeled T_e=$(T_{e1}^3 + T_{e2}^3)^{1/3}$ in Figure 5a).

If we assert that the cubic rule accurately represents a multilayer lithosphere when the normalized flexure, $w_0(t)/h_0$, differs from w_C by less than or equal to a fraction f of $w_E - w_C$ (i.e., the separation between the two horizontal lines in Figure 5a), then we can determine the upper bound timescale, t_u, on which the cubic rule applies. This leads to the following equation,

$$w_0(t)/h_0 - w_C = f(w_E - w_C), \tag{12}$$

where $w_0(t)$ is expressed

$$w_0(t)/h_0 = A_0^{(6)} e^{-t/\tau^{(6)}}/h_0 + A_0^{(7)}/h_0 - 1. \tag{13}$$

Substituting Equation 13 into Equation 12 and using Equation 11 for w_C, we have

$$t_u = t = ln\frac{1}{1-f}\tau^{(6)}. \tag{14}$$

This demonstrates that the upper bound timescale, t_u, on which the cubic rule applies, is only a fraction of $\tau^{(6)}$ depending on f, where f is the ratio of the deviation from the cubic rule ($w(t)/h_0 - w_C$) to the total deviation amplitude ($w_E - w_C$) which may be arbitrarily defined.

For example, if we choose f = 20% (i.e., 20% deviation from the bottom gray straight line to the top black straight line in Figure 5a), then $t_u = 0.223\tau^{(6)}$, and this illustrates that significant deviation from the cubic rule occurs before time reaches $\tau^{(6)}$. In Figure 6a, we present $\tau^{(6)}$ for Suites 1 and 2 with varying weak layer thicknesses, from which we can estimate the upper bound timescale, t_u, for each case. For example, in Case 1f with weak layer thickness 5 km, $\tau^{(6)} \sim 100$ Myr which leads to an upper bound timescale $t_u \sim 22$ Myr. For Case 1 with weak layer thickness equal to 20 km, $\tau^{(6)} \sim 2.3$ Myr which leads to an upper bound timescale $t_u \sim 0.5$ Myr. Alternatively, for f = 10%, $t_u = 0.105\tau^{(6)}$ which predicts even shorter upper bound timescales.

We also compute models with varying upper and lower competent layer thicknesses in Suite 3 with T_{e1} and T_{e2} equal to 20 and 50 km, in Suite 4 with 50 and 50 km, in Suite 5 with 10 and 10 km, and in Suite 6 with 50 and 100 km, respectively (Table 2). Results from all Suites 1–6 are summarized in Figures 6a and 6b. Figure 6a shows that $\tau^{(6)}$ is primarily controlled by the weak layer thickness but not the competent layer thicknesses, and that $\tau^{(6)}$ decreases from over 1 Gyr to less than 1 Myr as the weak layer thickness increases

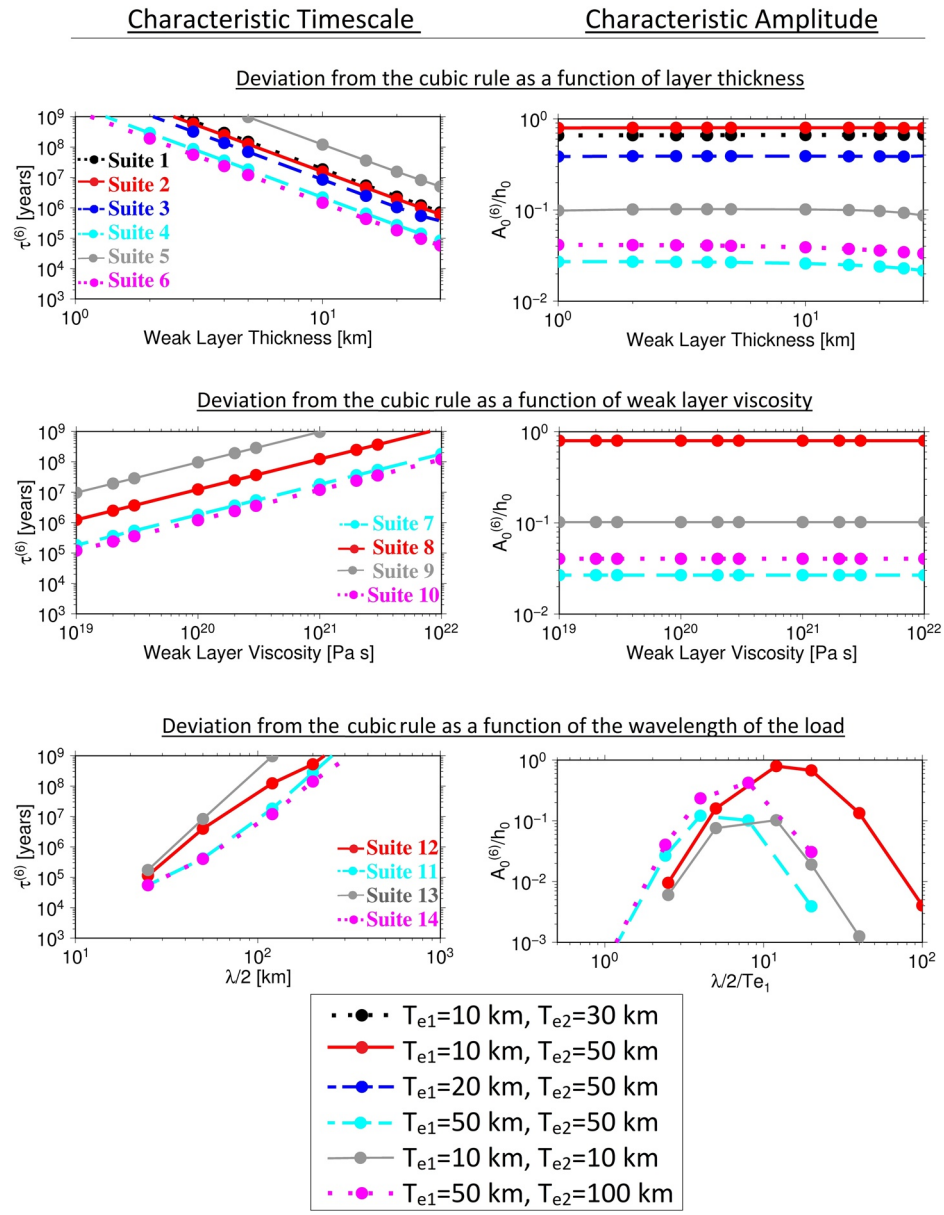

Figure 6. The characteristic timescale and amplitude of the sixth eigenmode or deviation from the cubic rule. The characteristics of the sixth eigenmode for multilayer lithospheres with (a and b) varying weak layer thickness, (c and d) varying weak layer viscosity, and (e and f) load wavelength. Note that the half-wavelength of the load is normalized by T_{e1} in (f) but not (e). The significance of the sixth eigenmode is that it represents the flexural deviation of a multilayer lithosphere from that predicted by the cubic rule. Also note that significant deviation from the cubic rule occurs on the upper bound timescale, t_u, which is a small fraction of $\tau^{(6)}$ (Equation 14).

from 1 to 30 km. We suggest that the intermediate weak layer decouples the lower competent layer from the surface load more efficiently when it is thicker. Furthermore, $\tau^{(6)}$ is also sensitive to the combined competent layer thickness or $(T_{e1}^3 + T_{e2}^3)^{1/3}$, such that $\tau^{(6)}$ decreases by a factor of ~100 as $(T_{e1}^3 + T_{e2}^3)^{1/3}$ increases from ~12 to ~100 km (Figure 6a, Table 2).

Figure 6b shows that the amplitude of the sixth eigenmode $A_0^{(6)}/h_0$ (i.e., the amplitude of the deviation from the cubic rule) is controlled by the competent layer thicknesses but not the weak layer thickness. On the one hand, the amplitude $A_0^{(6)}/h_0$ decreases for increasing T_{e1} (e.g., from ~0.85 to ~0.4 to ~0.03 for T_{e1} equal to 10 km, 20 km, and 50 km in Suites 2, 3, and 4, respectively) (Figure 6b, Table 2). This is easily understood if we consider that increasing T_{e1} always leads to reduced steady state flexure and, therefore, a smaller

deviation from the cubic rule upon relaxation of stresses in the deep lithosphere (i.e., $A_0^{(6)}/h_0$). In other words, the steady state flexure $|w_E| = 1-A_0^{(7)}/h_0$ decreases and $A_0^{(7)}/h_0$ increases as T_{e1} increases. Therefore, if we consider that the sum of the amplitudes of all eigenmodes, $\Sigma_{i=1}^{7} A_0^{(i)}/h_0$, is a constant (<1) defined by the instantaneous elastic response, then since the amplitudes of the first five eigenmode $A_0^{(1-5)}/h_0$ are consistent with the cubic rule and generally small, $A_0^{(6)}/h_0$ decreases as T_{e1} increases because $A_0^{(7)}/h_0$ increases with T_{e1}. Similarly, when T_{e1} is fixed, $A_0^{(7)}/h_0$ is also fixed (e.g., see Suites 1 and 2). On the other hand, the amplitude $A_0^{(6)}/h_0$ increases for increasing T_{e2} (e.g., from ~0.1 to ~0.65 to ~0.85 for T_{e2} equal to 10 km, 30 km, and 50 km in Suite 5, 1, and 2, respectively) (Figure 6b, Table 2). This is also easily understood if we consider that increasing T_{e2} suppresses the transient flexural response prior to the deviation from the cubic rule, but not after, such that deviation from the cubic rule is enhanced. In other words, increased T_{e2} suppresses $A_0^{(1-5)}/h_0$ but does not affect $A_0^{(7)}/h_0$, and therefore increases $A_0^{(6)}/h_0$ given $\Sigma_{i=1}^{7} A_0^{(i)}/h_0$, is a constant.

3.2.3. Effects of the Weak Layer Viscosity

We also test the sensitivity of the flexural response of a multilayer lithosphere to the viscosity of the intermediate weak layer. The weak layer viscosity is varied from 10^{19} to 10^{22} Pa s in a layer thickness equal to 5 km. We choose this weak layer thickness so that results can be easily scaled up or down to account for thinner or thicker weak layers based on Figure 6a. We also consider four different competent layer thickness combinations, where T_{e1} and T_{e2} are 50 and 50 km in Suite 7, 10, and 50 km in Suite 8, 10, and 10 km in Suite 9, and 50 and 100 km in Suite 10, respectively (Table 2). For reference, these competent layer thickness combinations are consistent with Suites 4, 2, 5, and 6, respectively.

The results are generally consistent with those for variation of the weak layer thickness, possibly because both properties of the weak layer have a similar influence on the degree of decoupling between the lower competent layer and the surface load. In particular, the effect of increasing the weak layer viscosity is similar to the effect of reducing the weak layer thickness such that $\tau^{(6)}$ is primarily controlled by weak layer viscosity (Figure 6c), and $A_0^{(6)}/h_0$ is again controlled by T_{e1} and T_{e2} (Figure 6d).

3.2.4. Effects of the Wavelength of the Load

Finally, we test the sensitivity of the results to the wavelength of the load. We vary the half-wavelength of the load from 25 to 1,000 km (Table 2). We consider four competent layer thickness combinations with T_{e1} and T_{e2} equal to 50 and 50 km in Suite 11, 10, and 50 km in Suite 12, 10, and 10 km in Suite 13, and 50 and 100 km in Suite 14, respectively (Table 2). For reference, the competent layer thickness combinations are consistent with those in Suites 7, 8, 9, and 10, respectively. The weak layer thickness is 5 km, and the weak layer viscosity is 10^{21} Pa s in all cases.

The value of $\tau^{(6)}$ ranges from ~10^5 years for load half-wavelengths of 25 km, to over 1 Gyr for load half-wavelengths ≥120 km (Figure 6e). This indicates that more rapid decoupling of the lower competent layer occurs for short-wavelength loads, and that reducing the wavelength of the load is similar in effect to increasing the thickness of the intermediate weak layer. For example, the 5 km weak layer is able to rapidly accommodate stresses associated with 25 km half-wavelength load, but the same 5 km weak layer is less efficient for loads with longer wavelengths, compared to which the weak layer is effectively thinner. In addition, $\tau^{(6)}$ is again somewhat sensitive to $(T_{e1}^{\ 3} + T_{e2}^{\ 3})^{1/3}$ in the same fashion as discussed previously (Figure 6).

The amplitude of the deviation from the cubic rule, $A_0^{(6)}/h_0$, is also sensitive to the wavelength of the load, and is maximal for $\lambda/2 \sim 10T_{e1}$ but diminishes to very small values for $\lambda/2 < T_{e1}$ and $100 \times T_{e1} < \lambda/2$ (i.e., at very short and very long wavelengths relative to T_{e1}) (Figure 6f). First, when $\lambda/2 < T_{e1}$, the relaxation of stress in the deep lithosphere (i.e., the sixth eigenmode and deviation from the cubic rule) has little effect on the surface because T_{e1} is capable of supporting the load to high degree. More specifically, the value of $A_0^{(6)}/h_0$ is small for $\lambda/2 < T_{e1}$ because the load is almost fully supported by T_{e1} at short-wavelengths, such that the steady state flexure is approximately zero (i.e., $w_E = A_0^{(7)}/h_0 - 1 \sim 0$), which requires that $A_0^{(7)}/h_0 \sim 1$ at the expense of all other eigenmodes (i.e., $A_0^{(6)}/h_0 \sim 0$). Second, when $100 \times T_{e1} < \lambda/2$, deviation from the cubic rule $A_0^{(6)}/h_0$ is small because the surface flexure generally reaches complete isostatic compensation of the load even on short timescales ($t \sim \tau^{(5)}$), which requires that $A_0^{(1-5)}$ be large and therefore both $A_0^{(6)}$ and $A_0^{(7)}$ be small given $\Sigma_{i=1}^{7} A_0^{(i)}/h_0$, is a constant (Zhong, 1997) (Figure 6f).

4. Discussion

We have demonstrated that the flexural response of a multilayer lithosphere is strongly dependent on the properties of the weak intermediate layer including its viscosity and thickness. This directly contradicts the reasoning behind the cubic rule, wherein the effective elastic thickness of a multilayer lithosphere is assumed to be a function of the competent layer thicknesses, only (Equation 3). The origin of the cubic rule, as described in the Introduction, is that the bending moment derived from the vertical integral of bending stresses is proportional to the elastic thickness cubed (T_e^3). What the cubic rule implicitly assumes is that each competent layer is subject to the same curvature as the uppermost competent layer, such that the sum for the total bending moment reduces to the sum for the total elastic thickness of a multilayer lithosphere. However, we have demonstrated in this study that the stress relaxes in the lower competent layer due to mechanical decoupling from the surface load. Therefore, the curvature of the lower competent layer reduces to much less than that of the surface layer, causing significant deviation from the cubic rule. The steady state flexure of a multilayer lithosphere in response to surface loads is controlled by the uppermost competent layer only, or $T_e = T_{e1}$, and the timescale to reach steady state is controlled by properties of the system which are discussed in more detail in the following.

The flexural response of a four-layer system (i.e., multilayer lithosphere) is controlled by seven eigenmodes. Our analysis revealed that the first five eigenmodes are associated with viscous relaxation of stress in the mantle which occurs on short timescales ($<10^5$ years for mantle viscosity of 10^{21} Pa s) and produces a flexural response that is consistent with the cubic rule. However, this response is transient and applies only for time less than an upper bound timescale, t_u, defined in Equation 14. The deviation from the cubic rule is caused by the sixth eigenmode which represents the decoupling effect of flow in the intermediate weak layer and the relaxation of stress in the lower competent layer on surface flexure. The characteristic timescale of the sixth eigenmode, $\tau^{(6)}$, is generally intermediate (Myr-Gyr) and primarily controlled by the thickness and viscosity of the weak layer (Figure 6). We emphasize that significant deviation from the cubic rule occurs for $t > t_u$ where t_u is generally a small fraction of $\tau^{(6)}$ (e.g., $t_u \sim 0.1\tau^{(6)}$–$0.2\tau^{(6)}$, Equation 14). Finally, the seventh eigenmode is associated with viscous relaxation of the competent upper crust, which occurs on very long timescales (10^{12} years for upper crustal viscosity of 10^{30} Pa s) and leads to complete isostatic compensation of the load.

Results show that if the intermediate weak layer is sufficiently thick and weak (i.e., thickness ≥5 km, viscosity ≤10^{21} Pa s) then deviation from the cubic rule occurs on rapid geological timescales (e.g., 10^5–10^8 years) for realistic lithospheric layer thicknesses and loads (Figure 6, Equation 14). The deviation is also sensitive to the wavelength of the load, where short-wavelength loads produce deviation on the shortest timescales, and intermediate-wavelengths ($\lambda/2 \sim 10T_{e1}$) produce the largest amplitude of deviation from the cubic rule, $A_0^{(6)}/h_0$ (Figure 6). Of greatest importance is that the steady state flexure of a multilayer lithosphere is controlled by the upper competent layer thickness, only, or $T_e = T_{e1}$, because the intermediate weak layer acts to decouple the lower competent layer from the surface load. We suggest that this new rule is more accurate and should be applied in place of the cubic rule in future studies of flexural systems that have achieved steady state.

4.1. Re-Interpreting Elastic Thickness in Continental Settings

It is generally expected that the T_e of continental lithosphere will correspond to the base of the mechanical lithosphere, which lies at the depth of the ~700°C isotherm based on laboratory-derived rheological laws (Brace & Kohlstedt, 1980). Previous studies recognized that this would be the case only for continental lithosphere that is fully mechanically coupled, and applied the cubic rule in continental settings with a weak lower crust (Burov & Diament, 1995; McNutt et al., 1988). However, we have shown in the present study that the cubic rule is not generally valid. In the following, we discuss the implications of re-interpreting elastic thickness in continental settings based on our new results.

In settings where the competent upper crust is much thinner than the mantle lithosphere ($T_{e1} << T_{e2}$), the cubic rule leads to significant misinterpretation and error because it predicts that $T_e = (T_{e1}^3 + T_{e2}^3)^{1/3} \sim T_{e2}$, while our new results indicate that $T_e = T_{e1}$. A mechanically competent upper crust that is thinner than the mantle lithosphere may arise in settings such as the Kazakh shield at the Northern Tien Shan, the

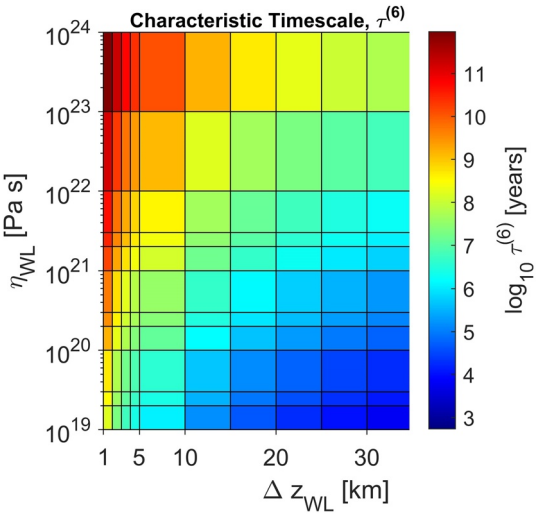

Figure 7. Summary of the characteristic timescale $\tau^{(6)}$ which governs deviation from the cubic rule and steady state flexure. The results from 110 analytic models are presented in terms of the timescale of the sixth eigenmode, $\tau^{(6)}$. All models have $T_{e1} = 10$ km and $T_{e2} = 50$ km, consistent with Suites 2, 8, and 12. The characteristic timescale may vary by a factor of ~10 if T_{e1} or T_{e2} are varied as in other Suites. Note that the deviation from the cubic rule occurs after ~0.1–0.2$\tau^{(6)}$, while steady state flexure is achieved after 2$\tau^{(6)}$–5$\tau^{(6)}$.

sub-Andean Range, and the Carpathians, where the continental lithosphere is old (>700 Myr) and the Moho is deep (>50 km). In such settings, the observational values of T_e coincide with the depth of the base of the competent upper crust (Burov & Diament, 1995), or $T_e = T_{e1}$, consistent with the newly derived rule in this study. This is a marked improvement compared to the cubic rule, which is inconsistent with the relatively small observational T_e (e.g., 20–40 km) at settings where the mantle lithosphere is quite thick (≥100 km), such as the Northern Tien Shan (Lü et al., 2020) and the sub-Andean range (Ward et al., 2016), although the thickness of the mantle lithosphere beneath the Carpathians is not generally agreed upon (Knapp et al., 2005).

In a multilayer lithosphere with thick upper crust compared to the mantle lithosphere ($T_{e1} >> T_{e2}$), the cubic rule makes predictions that are consistent with our new results because $T_e = (T_{e1}^3 + T_{e2}^3)^{1/3} \sim T_{e1}$. Similarly, in multilayer lithospheres where $T_{e1} \sim T_{e2}$, the cubic rule makes somewhat reasonable predictions because $T_e = (T_{e1}^3 + T_{e2}^3)^{1/3} = 2^{1/3}T_{e1}$, which comprises relatively modest error (26%). A mechanically competent upper crust of equal or greater thickness than the mantle lithosphere may arise in young (<400 Ma) continental lithosphere and older continental lithosphere that has been significantly warmed from below (i.e., thermally rejuvenated). Observationally inferred estimates of T_e are consistent with the depth to the base of the mechanically competent crust and the 200°–400°C isotherm depth (Burov & Diament, 1995) in young continental settings such as the Eastern Alps (Karner & Watts, 1983), the Transverse Ranges (Sheffels & McNutt, 1986), the Apennines (Kruse & Royden, 1994), the Pamirs (Burov et al., 1990), Lake Bonneville and Lake Hamilton (Watts, 1992), and these observations are consistent with both the new results of this study and the cubic rule.

The cubic rule makes correct predictions for flexural systems in which the transient solution persists (i.e., $t < t_u$, Equation 14), which may be relevant in continental settings where the loading process is recent or ongoing. For example, the Zagros Mountains continue to experience uplift today due to collision of the Arabian plate with Eurasia, and Lake Baikal is 25–30 Ma, a timescale on which the transient solution (i.e., the cubic rule) may persist depending on the properties of the weak lower crust. In these settings, the observationally inferred estimates of T_e are intermediate between the cubic rule and the new rule derived herein, $(T_{e1}^3 + T_{e2}^3)^{1/3} > T_e > T_{e1}$, which may indicate that relaxation of the mantle lithosphere is ongoing. In particular, observationally inferred estimates of elastic thickness are $T_e \sim 50$ km at the Zagros mountains and North Baikal Lake where the base of the mechanically competent crust is ~40 km deep and the base of the mantle lithosphere is ~135 km deep (Burov & Diament, 1995).

Glacial isostatic adjustment (GIA) is generally associated with very recent loading (e.g., $<25 \times 10^3$ years), such that we would not expect the flexural response of a multilayer lithosphere to have reached steady state (i.e., $T_e = T_{e1}$ applies) unless the weak lower crust is quite weak and/or quite thick. In Figure 7, we present the characteristic timescale to reach steady state flexure, $\tau^{(6)}$, for a broad range of weak layer properties. Note that the timescale to achieve steady state flexure is generally longer than $\tau^{(6)}$ (e.g., 2$\tau^{(6)}$–5$\tau^{(6)}$), similar to how the timescale of deviation from the cubic rule is generally shorter than $\tau^{(6)}$ (e.g., 0.223$\tau^{(6)}$, Equation 14). To reach steady state flexure on the timescale associated with GIA (25×10^3 years) such that $T_e = T_{e1}$ applies would require a weak lower crustal thickness ≥20 km and weak lower viscosity ≤10^{20} Pa s, for a load with $\lambda/2 = 120$ km, $T_{e1} = 10$ km and $T_{e2} = 50$ km. Note that this timescale would also increase for increasing wavelength of the load, and could either increase or decrease by ×10 depending on T_{e1} and T_{e2} (refer to Figure 6).

Migration of foreland basins and the associated flexural bulge may also comprise evidence of the effects of a weak lower crust on flexure in the sediment stratigraphy (DeCelles & Giles, 1996; Patton & O'Connor, 1988). In particular, if stress relaxation occurs in the mantle lithosphere due to the existence of a weak lower crust, then the effective elastic thickness of the system would reduce with time such that the forebulge would

migrate toward the load. In general, forebulge migration away from the load (i.e., craton-ward) is more commonly observed because loads associated with orogens often advance (e.g., Currie, 1997; Price & Hatcher, 1983; Roddaz et al., 2005; Ussami et al., 1999; White et al., 2002). However, instances in which the forebulge migrates toward the orogen or load include the foreland basin of Alberta during the Cretaceous (Plint et al., 1993), the Appalachian basin during the Devonian (Dever et al., 1977; Quinlan & Beaumont, 1984), the east-Ural basin during the Carboniferous (Proust et al., 1998), and the Llanos basin during the Eocene (Bayona et al., 2007). While previous studies have attributed load-ward migration of the forebulge to lateral variations in flexural strength of the lithosphere or basin formation dynamics, the work presented herein is the first to demonstrate that vertical variation in lithospheric strength (e.g., a weak lower crust) is also capable of producing lateral migration of a forebulge.

An additional implication of the newly derived rule, $T_e = T_{e1}$, is that small estimates of T_e in continental settings may not necessarily indicate a thin mantle lithosphere if a weak lower crust is present. It is of great importance that seismic tomography be used in combination with flexural studies to understand the structure of continental lithosphere, because estimates of T_e that are consistent with the thickness of the mechanically competent upper crust cannot be used independently to discriminate between a jelly sandwich and a crème brûlée configuration (Burov, 2015). For example, seismic tomography indicates that old, cold, and thick mantle lithosphere does not exist at Lake Bonneville (Austermann et al., 2019; Shen et al., 2013). We propose that the presence of a weak lower crust could be partially responsible for the low inferred values of T_e at coronae (Russell & Johnson, 2021) despite the stagnant-lid convection style of Venus, but future missions will be required to test this hypothesis using seismic tomography.

In this study we have considered only surface loads although subsurface loads may also exist in Earth and planetary systems. For loads that are internal to the upper crust, we expect the flexural response to be equivalent to that demonstrated for surface loads, that is, the flexural response will be controlled by the upper crust only, or $T_e = T_{e1}$. However, if a multilayer lithosphere is acted upon by a load that is internal to the mantle lithosphere, or imposed on the base of the mantle lithosphere, then we expect that the flexural response will be controlled by the mantle lithosphere only, or $T_e = T_{e2}$, and that the stress associated with the load will not be transmitted to the upper crust or surface on long geologic timescales (e.g., Bindschadler & Parmentier, 1990).

Finally, the results presented in this study are subject to the limitation of complete crustal extrusion which may occur in real Earth systems if the difference in flexure between two competent layers exceeds the thickness of the intermediate weak layer. If the two competent layers come into contact with each other completely, then the total elastic thickness is the sum of the thicknesses of the two layers, that is, $T_e = T_{e1} + T_{e2}$. If the two competent layers come into contact only at some isolated patches, the effective elastic thickness is likely between $T_e = T_{e1} + T_{e2}$ and T_{e1}. In the latter case, the numerical models can be reformulated to account for the partial contacts between the two layers, while our analytical models are no longer applicable. While our new result appears to improve understanding of flexure at the Kazakh Shield, the Northern Tien Shan, and the sub-Andean Range, we acknowledge that flexure in systems with complete crustal extrusion would differ.

5. Conclusions

The response of a multilayer lithosphere with an intermediate weak layer to a surface load is investigated using 2D viscoelastic loading models. Results show that the steady state surface flexure is controlled by the uppermost mechanically competent layer, only, or $T_e = T_{e1}$. This is because the intermediate weak layer acts to decouple the surface load from the lower competent layer. As a result, stresses relax in the lower competent layer which eventually does not support the surface load at all. The timescale to reach steady state is controlled primarily by the properties of the intermediate weak layer and the geometry of the load, where greater weak layer thickness, lower weak layer viscosity, and shorter load-wavelengths produce steady state more rapidly. The timescale to reach steady state is as short as $\sim 5 \times 10^5$–10^7 years for many of the geologically reasonable rheological parameters (weak layer viscosity $\geq 10^{19}$ Pa s) and structures (weak layer thickness ≥ 5 km, load wavelength $\lambda = 240$ km) tested herein (Figures 6 and 7), and deviation from the cubic rule

occurs much sooner. We therefore consider our new result, $T_e = T_{e1}$, to be geologically relevant and a significant improvement to our understanding of flexural dynamics compared to the cubic rule. The improvement of this new rule $T_e = T_{e1}$ compared to the cubic rule is also corroborated by observational estimates of T_e that are consistent with the depth to the base of the mechanically competent upper crust (i.e., $T_e = T_{e1}$) in the Kazakh Shield at Northern Tien Shan and the sub-Andean Range. Finally, the amplitude of the flexural deviation from the cubic rule is controlled primarily by the competent layer thicknesses and the wavelength of the load, such that the revisions to previous studies which used the cubic rule are most significant in geologic settings with intermediate load wavelengths ($\lambda/2 \sim 10T_{e1}$) and thick mantle lithosphere ($T_{e2} >> T_{e1}$).

Data Availability Statement

The analytic and numerical codes used to produce the data in this study will be made available upon request or can be downloaded from https://doi.org/10.6084/m9.figshare.14226716.v1.

Acknowledgments
The authors are grateful for support from NSF EAR-1940026 without which this research would not be possible. A big thanks to Craig Jones and Peter Molnar for productive discussions and feedback, and to J. Perry-Houts and P. McGovern for their constructive reviews.

References

Austermann, J., Chen, C. Y., Lau, H. C. P., Maloof, A. C., & Latychev, K. (2019). Constraints on mantle viscosity and Laurentide ice sheet evolution from pluvial paleolake shorelines in the western United States. *Earth and Planetary Science Letters*, *532*, 116006. https://doi.org/10.1016/j.epsl.2019.116006

Bayona, G., Jaramillo, C., Rueda, M., Reyes-Harker, A., & Torres, V. (2007). Paleocene-middle Miocene flexural-margin migration of the nonmarine llanos foreland basin of Colombia. *Ciencia, Tecnologia y Futuro*, *3*, 51–70.

Bellas, A., & Zhong, S. J. (2021). Seismic strain rate and flexure at the Hawaiian Islands constrain the frictional coefficient. *Geochemistry, Geophysics, Geosystems*, *22*, e2020GC009547. https://doi.org/10.1029/2020GC009547

Bellas, A., Zhong, S. J., & Watts, A. B. (2020). Constraints on the rheology of the lithosphere from flexure of the Pacific Plate at the Hawaiian Islands. *Geochemistry, Geophysics, Geosystems*, *21*, e2019GC008819. https://doi.org/10.1029/2019GC008819

Bindschadler, D. L., & Parmentier, E. M. (1990). Mantle flow tectonics: The influence of a ductile lower crust and implications for the formation of topographic uplands on Venus. *Journal of Geophysical Research*, *95*(B13), 21329–21344. https://doi.org/10.1029/jb095ib13p21329

Bird, P. (1991). Lateral extrusion of lower crust from under high topography, in the isostatic limit. *Journal of Geophysical Research*, *96*(B6), 10275–10286. https://doi.org/10.1029/91jb00370

Brace, W. F., & Kohlstedt, D. L. (1980). Limits on lithospheric stress imposed by laboratory experiments. *Journal of Geophysical Research*, *85*, 6248–6252. https://doi.org/10.1029/jb085ib11p06248

Burov, E. B. (2015). Chapter 6.03: Plate rheology and mechanics. In *Treatise on Geophysics*. (2nd ed., pp. 95–152). Elsevier. https://doi.org/10.1016/b978-0-444-53802-4.00112-3

Burov, E. B., & Diament, M. (1995). The effective elastic thickness (Te) of continental lithosphere: What does it really mean? *Journal of Geophysical Research*, *100*(B3), 3905–3927. https://doi.org/10.1029/94jb02770

Burov, E. B., Kogan, M. G., Lyon-Caen, H., & Molnar, P. (1990). Gravity anomalies, the deep structure, and dynamic processes beneath the Tien Shan. *Earth and Planetary Science Letters*, *96*, 367–383. https://doi.org/10.1016/0012-821x(90)90013-n

Chen, W. P., & Molnar, P. (1983). Focal depths of intracontinental and intraplate earthquakes and their implications for the thermal and mechanical properties of the lithosphere. *Journal of Geophysical Research*, *88*(B5), 4183–4214. https://doi.org/10.1029/jb088ib05p04183

Clark, M., & Royden, L. (2000). Topographic ooze: Building the eastern margin of Tibet by lower crustal flow. *Geology*, *28*, 703–706. https://doi.org/10.1130/0091-7613(2000)028<0703:tobtem>2.3.co;2

Currie, B. S. (1997). Sequence stratigraphy of nonmarine Jurassic-Cretaceous rocks, central Cordilleran foreland- basin system. *GSA Bulletin*, *109*(9), 1206–1222. https://doi.org/10.1130/0016-7606(1997)109<1206:ssonjc>2.3.co;2

DeCelles, P. G., & Giles, K. (1996). Foreland basin systems. *Basin Research*, *8*, 105–123. https://doi.org/10.1046/j.1365-2117.1996.01491.x

Dever, G. R., Hoge, H., Hester, N., & Ettensohn, F. (1977). *Stratigraphic evidence for late Paleozoic tectonism in northeastern Kentucky*. Lexington, KY: American Association of Petroleum Geologists, Eastern Section.

Garcia, E. S., Sandwell, D. T., & Bassett, D. (2019). Outer trench slope flexure and faulting at Pacific basin subduction zones. *Geophysical Journal International*, *218*, 708–728. https://doi.org/10.1093/gji/ggz155

Goetze, C., & Evans, B. (1979). Stress and temperature in the bending lithosphere as constrained by experimental rock mechanics. *Geophysical Journal International*, *59*, 463–478. https://doi.org/10.1111/j.1365-246x.1979.tb02567.x

Hager, B., & O'Connell, R. (1981). A simple global model of plate dynamics and mantle convection. *Journal of Geophysical Research*, *86*(B6), 4843–4867. https://doi.org/10.1029/jb086ib06p04843

Karner, G. D., & Watts, A. B. (1983). Gravity anomalies and flexure of the lithosphere at mountain ranges. *Journal of Geophysical Research*, *88*(B12), 10449–10477. https://doi.org/10.1029/jb088ib12p10449

Knapp, J. H., Knapp, C. C., Raileanu, V., Matenco, L., Mocanu, V., & Dinu, C. (2005). Crustal constraints on the origin of mantle seismicity in the Vrancea Zone, Romania: The case for active continental lithospheric delamination. *Tectonophysics*, *410*, 311–323. https://doi.org/10.1016/j.tecto.2005.02.020

Kruse, S. E., & Royden, L. H. (1994). Bending and unbending of an elastic lithosphere: The Cenozoic history of the Apennine and Dinaride foredeep basins. *Tectonics*, *13*, 278–302. https://doi.org/10.1029/93tc01935

Lü, Z., Gao, H., & Lei, J. (2020). New insight into crustal and lithospheric variability beneath the central Tien Shan (NW China) revealed by P-wave receiver functions. *Journal of Asian Earth Sciences*, *189*, 104187. https://doi.org/10.1016/j.jseaes.2019.104187

McNutt, M., Diament, M., & Kogan, M. G. (1988). Variations of elastic plate thickness at continental thrust belts. *Journal of Geophysical Research*, *93*, 8825–8838. https://doi.org/10.1029/jb093ib08p08825

McNutt, M. K. (1984). Lithospheric flexure and thermal anomalies. *Journal of Geophysical Research*, *89*(11), 11180–11194. https://doi.org/10.1029/jb089ib13p11180

McNutt, M. K., & Menard, H. W. (1982). Constraints on yield strength in the oceanic lithosphere derived from observations of flexure. *Geophysical Journal International*, *71*(2), 363–394. https://doi.org/10.1111/j.1365-246x.1982.tb05994.x

Mueller, S., & Phillips, R. J. (1995). On the reliability of lithospheric constraints derived from models of outer-rise flexure. *Geophysical Journal International*, *123*(3), 887–902. https://doi.org/10.1111/j.1365-246x.1995.tb06896.x

Patton, T. L., & O'Connor, S. J. (1988). Cretaceous flexural history of northern Oman mountain foredeep, United Arab Emirates. *AAPG Bulletin*, *72*, 797–809.

Paulson, A., Zhong, S. J., & Wahr, J. (2005). Modeling post-glacial rebound with lateral viscosity variations. *Geophysical Journal International*, *163*, 357–371. https://doi.org/10.1111/j.1365-246x.2005.02645.x

Plint, A. G., Hart, B., & Donaldson, W. S. (1993). Lithospheric flexure as a control on stratal geometry and facies distribution in Upper Cretaceous rocks of the Alberta foreland basin. *Basin Research*, *5*, 69–77. https://doi.org/10.1111/j.1365-2117.1993.tb00058.x

Price, R. A., & Hatcher, R. D. (1983). Tectonic significance of similarities in the evolution of the Alabama-Pennsylvania Appalachians and the Alberta-British Columbia Canadian Cordillera. In Hatcher, R. D., Williams,H. (Eds.), & Zietz, I. (Eds), *Contributions to the tectonics and Geophysics of mountain Chains*. (Vol. 158, pp. 149–160). Memoirs–Geological Society of America. https://doi.org/10.1130/mem158-p149

Proust, J. N., Chuvashov, B. I., Vennin, E., & Boisseau, T. (1998). Carbonate platform drowning in a foreland setting: The mid-Carboniferous platform in western Urals (Russia). *Journal of Sedimentary Research*, *68*, 1175–1188. https://doi.org/10.2110/jsr.68.1175

Quinlan, G. M., & Beaumont, C. (1984). Appalachian thrusting, lithospheric flexure, and the Paleozoic stratigraphy of the eastern interior of North America. *Canadian Journal of Earth Sciences*, *21*, 973–996. https://doi.org/10.1139/e84-103

Roddaz, M., Baby, P., Brusset, S., Hermoza, W., & Maria Darrozes, J. (2005). Forebulge dynamics and environmental control in Western Amazonia: The case study of the Arch of Iquitos (Peru). *Tectonophysics*, *399*, 87–108. https://doi.org/10.1016/j.tecto.2004.12.017

Royden, L. H., Burchfiel, B. C., King, R. W., Wang, E., Chen, Z., Shen, F., & Liu, Y. (1997). Surface deformation and lower crustal flow in eastern Tibet. *Surface deformation and lower crustal flow in Eastern Tibet*, *276*, 788–790. https://doi.org/10.1126/science.276.5313.788

Russell, M., & Johnson, C. L. (2021). Evidence for a locally thinned lithosphere associated with volcanism at Aramaiti Corona, Venus. *Journal of Geophysical Research: Planets*, *126*, e2020JE006783. https://doi.org/10.1029/2020JE006783

Shapiro, N. M., Ritzwoller, M. H., Molnar, P., & Levin, V. (2004). Thinning and Flow of Tibetan Crust Constrained by Seismic Anisotropy. *Science*, *305*, 233–236. https://doi.org/10.1126/science.1098276

Sheffels, J. G., & McNutt, M. (1986). Role of subsurface loads and regional compensation in the isostatic balance of the Transverse Ranges, California: Evidence of intracontinental subduction. *Journal of Geophysical Research*, *92*, 6419–6431. https://doi.org/10.1029/jb091ib06p06419

Shen, W., Ritzwoller, M. H., & Schulte-Pelkum, V. (2013). A 3-D model of the crust and uppermost mantle beneath the Central and Western US by joint inversion of receiver functions and surface wave dispersion. *Journal of Geophysical Research: Planets*, *118*, 262–276. https://doi.org/10.1029/2012JB009602

Turcotte, D. L., & Schubert, G. (1982). *Geodynamics*. Cambridge University Press.

Ussami, N., Shiraiwa, S., & Dominguez, J. M. L. (1999). Basement reactivation in a sub-Andean foreland flexural bulge: The Pantanal wetland, SW Brazil. *Tectonics*, *18*, 25–39. https://doi.org/10.1029/1998tc900004

Walcott, R. I. (1970). Flexure of the lithosphere at Hawaii. *Tectonophysics*, *9*, 435–446. https://doi.org/10.1016/0040-1951(70)90056-9

Ward, K. M., Zandt, G., Beck, S. L., Wagner, L. S., & Tavera, H. (2016). Lithospheric structure beneath the northern Central Andean Plateau from the joint inversion of ambient noise and earthquake-generated surface waves. *Journal of Geophysical Research: Planets*, *121*, 8217–8238. https://doi.org/10.1002/2016JB013237

Watts, A. B. (1992). The effective elastic thickness of the lithosphere and the evolutions of foreland basins. *Basin Research*, *4*, 169–178. https://doi.org/10.1111/j.1365-2117.1992.tb00043.x

Watts, A. B. (2001). *Isostasy and flexure of the lithosphere* (p. 472). Cambridge: Cambridge University Press. https://doi.org/10.1136/bmj.323.7311.472

White, T., Furlong, K., & Arthur, M. (2002). Forebulge migration in the Cretaceous wester interior of the central United States. *Basin Research*, *14*, 43–54. https://doi.org/10.1046/j.1365-2117.2002.00165.x

Zhong, S. J. (1997). Dynamics of crustal compensation and its influences on crustal isostasy. *Journal of Geophysical Research*, *102*(B7), 14287–15299. https://doi.org/10.1029/97jb00956

Zhong, S. J., Paulson, A., & Wahr, J. (2003). Three-dimensional finite-element modelling of Earth's viscoelastic deformation: Effects of lateral variations in lithospheric thickness. *Geophysical Journal International*, *155*, 679–695. https://doi.org/10.1046/j.1365-246x.2003.02084.x

Zhong, S. J., & Watts, A. B. (2013). Lithospheric deformation induced by loading of the Hawaiian Islands and its implications for mantle rheology. *Journal of Geophysical Research*, *118*(11), 6025–6048. https://doi.org/10.1002/2013jb010408